THE JOURNAL OF PHYSICAL CHEMISTRY A
A JOURNAL OF THE AMERICAN CHEMICAL SOCIETY

pubs.acs.org/JPCA Article

# Torsional Profiles of Thiophene and Furan Oligomers: Probing the Effects of Heterogeneity and Chain Length

Morgan A. Perkins, Laura M. Cline, and Gregory S. Tschumper*

Cite This: https://doi.org/10.1021/acs.jpca.1c04714 Read Online



**ABSTRACT:** A systematic analysis of the torsional profiles of 55 unique oligomers composed of two to four thiophene and/or furan rings ($n$ = 2 to 4) has been conducted using three density functional theory (DFT) methods along with MP2 and three different coupled-cluster methods. Two planar or quasi-planar minima were identified for each $n$ = 2 oligomer system. In every case, the torsional angle ($\tau$) between the heteroatoms about the carbon−carbon bond connecting the two rings is at or near 180° for the global minimum and 0° for the local minimum, referred to as *anti* and *syn* conformations, respectively. These oligomers have rotational barrier heights ranging from *ca.* 2 kcal mol$^{-1}$ for 2,2′-bithiophene to 4 kcal mol$^{-1}$ for 2,2′-bifuran, based on electronic energies computed near the CCSD(T) complete basis set (CBS) limit. The corresponding rotational barrier for the heterogeneous 2-(2-thienyl)furan counterpart falls approximately halfway between those values. The energy differences between the minima are approximately 2 and 0.4 kcal mol$^{-1}$ for the homogeneous 2,2′-bifuran and 2,2′-bithiophene, respectively, whereas the energy difference between the planar local and global minima (at $\tau$ = 0 and 180°, respectively) is only 0.3 kcal mol$^{-1}$ for 2-(2-thienyl)furan. Extending these three oligomers by adding one or two additional thiophene and/or furan rings resulted in only minor changes to the torsional profiles when rotating around the same carbon−carbon bond as the two-ring profiles. Relative energy differences between the *syn* and *anti* conformations were changed by no more than 0.4 kcal mol$^{-1}$ for the corresponding $n$ = 3 and 4 oligomers, while the rotational barrier height increased by no more than 0.8 kcal mol$^{-1}$.

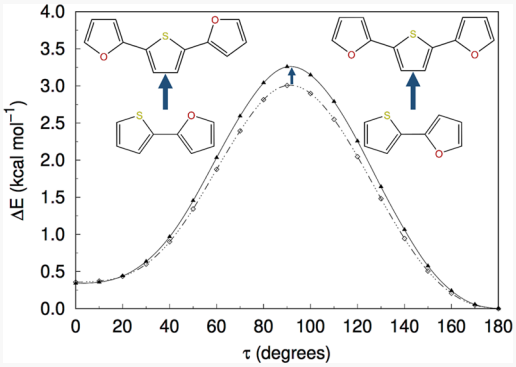


## 1. INTRODUCTION

Since the early development of semiconducting films made from organic polymers, the use of organic materials as an alternative to inorganic materials for building optoelectronic devices has risen in popularity.[1−3] These conjugated, semiconducting materials typically take the form of an oligomer, polymer, or small molecule. Compared to their inorganic counterparts, organic materials are flexible, naturally abundant, more easily tunable via synthesis (allowing for greater control over resulting optical and mechanical properties of devices) and are generally more cost effective to produce.[4,5] Ideal semiconducting systems should exhibit $\pi$ conjugation, be rigid to interconversion, and have tight solid-state packing. These materials can be used in the fabrication of organic light-emitting diodes (OLEDs), organic field-effect transistors (OFETs), organic photovoltaics (OPVs), solar cells, and biochemical sensors. A material that is sufficient for one purpose, like the production and transportation of charge, is not necessarily good for another, like releasing a photon.[5] Therefore, understanding the characteristics of molecular building blocks themselves, such as how features like structural properties relate to overall device properties, provides a better guide for researchers in the design and improvement of these materials. Two popular building blocks, heterocycles thiophene (Tn) and furan (Fn), are depicted in Figure 1.

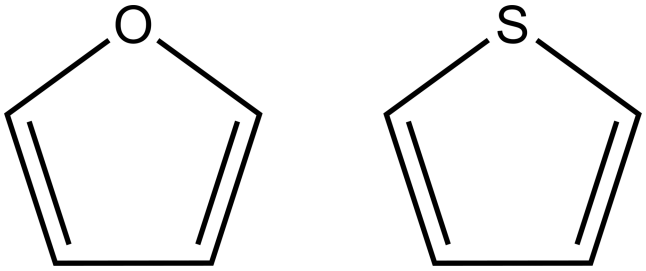


**Figure 1.** Popular heterocyles used as building blocks for organic semiconducting materials: furan (Fn) on the left and thiophene (Tn) on the right.

Oligo- and polythiophenes are among some of the earliest materials used in the development of organic-based semiconductors[6−9] and remain the focus of a significant portion of the research done today.[10−14] Thiophene-based semiconduc-

**Received:** May 28, 2021
**Revised:** June 24, 2021

  

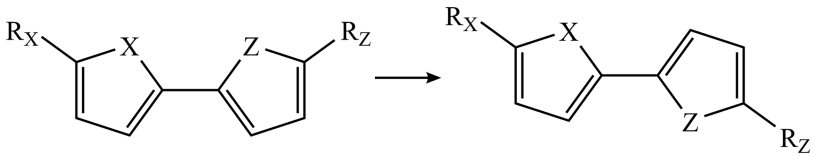


| | | |
|---|---|---|
| $n = 2$ | $R_X = H$ | $R_Z = H$ |
| $n = 3$ | $R_X = Fn, Tn$ | $R_Z = H$ |
| $n = 4$ | $R_X = Fn, Tn$ | $R_Z = Fn, Tn$ |

**Figure 2.** General structure of oligomers analyzed in this study, where the XCCZ torsional angle varied in the scans ($\tau$) is depicted at 0° (left) and 180° (right).

tors have many properties that make them attractive for use in optoelectronic devices. They are easily obtained from natural sources (such as plants of the Asteraceae family)[15] and are fairly easy to synthetically modify. However, working with thiophene-based materials is not without challenge. Their low solubility in organic solvents often requires the addition of solubilizing groups, reducing the material's packing efficiency.[4,16] Their electronic properties, specifically luminescence, are far from efficient, and additional structures, such as electron acceptors, must often be incorporated into thiophene-based systems to increase their electronic efficiency.[17] Given the synthetic challenges and low luminescent capabilities, these systems remain far from ideal.

The closely related heterocycle furan has long been incorporated into the framework of more widely studied organic semiconducting materials, such as oligo- and polythiophenes.[18−20] Initially, pure poly- and oligofurans were rarely used due to the difficulty of synthesizing the materials and their instability in oxidative conditions.[21,22] After these challenges were overcome, furan-based materials were found to have a variety of useful properties, including tight solid-state packing. Compared to oligothiophenes, oligofurans have a lower internal reorganization energy, are more soluble, and are highly fluorescent.[21,23,24] The hole mobility, a measure of the level of semiconducting potential, was found to be 1.6 times higher for a furan system than an equivalent thiophene system.[22] Similar to oligothiophenes, they are readily obtained from renewable resources such as plant biomass.[25]

Both furan- and thiophene-based systems have their merits, and the investigation of a hybrid system consisting of both furan and thiophene is particularly interesting because of the potential for improvements in structural and electronic properties such as stacking distance, solubility, and charge transport. Varying the identity and conformation of the heteroatoms present on heterocycles in a chain can drastically alter the electronic, optical, and physical properties of the system.[26−30] In particular, switching from an all thiophene to an alternating hybrid system reduces intersystem crossing (leading to better electronic properties) due to oxygen's reduced spin-orbit coupling.[29] In addition, oxygen's smaller radius (when compared to sulfur) results in a more tightly packed system with a denser backbone. This decrease in the intermolecular spacing makes the system a more efficient electron carrier. Furthermore, the presence of furan rings can improve the solubility of the system and decrease the need for solubilizing groups.

Computational and theoretical analyses have been utilized along with experimental methods to study electronic and optical properties of both thiophene- and furan-based materials.[27,31−37] A significant amount of research focuses on short oligomers (made up of as few as two or three heterocycles), which allows researchers to probe structural properties and torsional profiles of these systems in greater detail.[26,28,35,36,38−61] Density functional theory (DFT) techniques are frequently used to characterize these short oligomers, often after calibrating the DFT methods against experimental or *ab initio* quantum mechanical electronic structure methods. Some of the most rigorous studies have used coupled-cluster methods, such as CCSD, CCSD(T), and even CCSDT, to characterize the torsional profiles of the smallest oligomers with only two rings. These include the homogeneous 2,2′-bifuran and 2,2′-bithiophene systems[57] (denoted Fn−Fn and Tn−Tn, respectively) as well as the heterogeneous 2-(2-thienyl)furan system (Tn−Fn),[55] where the dash in this notation emphasizes the bond about which the torsional profile is examined. The generic structure of these three oligomers is depicted for $n = 2$ in Figure 2, where $R_X$=$R_Z$=H, while X=Z=O corresponds to Fn−Fn, X=Z=S corresponds to Tn−Tn, and X=S and Z=O corresponds to Tn−Fn.

The present study will extend this previous computational work in two important ways. The conformational energetics of Tn−Fn will be computed near the CCSD(T) complete basis set (CBS) limit, similar to the work that has already been done for Fn−Fn and Tn−Tn. Less demanding computational approaches capable of reproducing coupled-cluster benchmark torsional profiles for those three dimers will then be used to examine how the torsional profiles of the oligomers change as the number of rings ($n$) increases from two rings to three or four rings, as depicted schematically in Figure 2.

## 2. COMPUTATIONAL DETAILS

Full geometry optimizations and harmonic vibrational frequency computations (used to identify structures as minima or transition states) were performed on the Fn−Fn, Tn−Tn, and Tn−Fn systems using second-order Møller−Plesset Perturbation theory (MP2)[62] and three different DFT methods: the hybrid functional B3LYP,[63−65] the long-range corrected hybrid functional $\omega$B97XD,[66] and the hybrid meta-generalized gradient approximation (GGA) functional M06-2X.[67] These DFT methods have been selected because they have been reported to provide reliable structures and energetics for similar systems.[57,59,61] Constrained geometry optimizations, referred to as relaxed scans, were also performed


https://doi.org/10.1021/acs.jpca.1c04714
J. Phys. Chem. A XXXX, XXX, XXX−XXX

on all three of the two-ring systems using the same series of methods. For the relaxed scans, a single torsional angle between heteroatoms X and Z about the central carbon−carbon bond was varied from 0 to 180° in 10° increments while allowing all other parameters to fully optimize. Single-point coupled-cluster computations with full single and double excitations and perturbative triple excitations (CCSD(T))[68−70] were performed on the MP2 structures obtained from the full geometry optimizations and relaxed scans. All DFT, MP2, and CCSD(T) computations used Dunning's correlation consistent basis set, cc-pVTZ[71,72] (denoted VTZ). The torsional profiles of Tn−Tn and Tn−Fn were also computed with the cc-pV(T+*d*)Z basis set. That data has been relegated to the Supporting Information because the additional tight *d*-functions did not have a significant effect on the results. Additional single-point computations were carried out on the two-ring systems using two explicitly correlated CCSD(T) methods: CCSD(T)-F12[73,74] and a local method with pair natural orbitals, PNO-LCCSD(T)-F12.[75,76] The triple energy contribution was not scaled for either method. CCSD(T)-F12 single points were performed on all MP2 structures obtained from full geometry optimizations (similar to CCSD(T) single points) and on just three structures from MP2 relaxed scans ($\tau$ = 0, 90, and 180°), while PNO-LCCSD(T)-F12 single points were performed on all of the same MP2 structures as CCSD(T) single points. For these explicitly correlated methods, cc-pV*X*Z-F12 atomic orbital (AO) basis sets[77] (denoted as V*X*Z-F12, where *X* = T for PNO-LCCSD(T)-F12 and *X* = T, Q for CCSD(T)-F12) were utilized along with the default resolution of the identity and density fitting basis sets[78−80] defined in Molpro.[81,82]

For larger three- and four-ring oligomers ($n$ = 3 and 4, respectively), the $\omega$B97XD density functional method was used to characterize the structures instead of the MP2 method. In the case of $n$ = 3, $\omega$B97XD relaxed scans were performed with the VTZ basis set employing two constrained parameters: $\tau$ and an additional torsional angle, denoted as $\tau_X$, between heteroatom X and the heteroatom on the ring at the $R_X$ position (Figure 2). The torsional angle $\tau$ was varied as before, from 0 to 180° in 10° increments, while $\tau_X$ was fixed at either 0 or 180° for each $\tau$ value. The notation used to identify each three-ring oligomer is an extension of the two-ring notation. The $R_X$ substituent is prepended to the pair of rings defining the torsional angle ($\tau$) for the scan, while the value of $\tau_X$ is indicated as a subscript to $R_X$, creating labels such as $Fn_0$ Fn−Fn and $Tn_{180}$ Tn−Fn. Note that for these systems where $n$ = 3, $R_Z$ = H and is not explicitly written out. PNO-LCCSD(T)-F12/VTZ-F12 single-point energies were computed for all of the $\omega$B97XD scan points, while CCSD(T)/VTZ and CCSD(T)-F12/VTZ-F12 single-point computations were performed exclusively on the $\tau$ = 0, 90, and 180° $\omega$B97XD scan points.

For four-ring oligomers, constrained optimizations using $\omega$B97XD with the VTZ basis set were run only on structures with a $\tau$ value of 0, 90, or 180°. Each of those structures had two additional frozen torsional angles, $\tau_X$ and $\tau_Z$ (where $\tau_Z$ is the torsional angle between heteroatom Z and the heteroatom on the ring at the $R_Z$ position in Figure 2), which were fixed at either 0 or 180°. For the four-ring notation, the $R_X$ and $R_Z$ substituents are prepended and appended, respectively, to the two-ring notation and the $\tau_X$ and $\tau_Z$ values are given as subscripts, leading to labels such as $Fn_0$ Fn−Fn $Tn_{180}$. PNO-LCCSD(T)-F12 and CCSD(T) single-point computations were performed on all of the four-ring $\omega$B97XD structures obtained from relaxed scans. All methods used to study the four-ring systems utilized the same basis sets as for the three-ring systems.

For this work, spherical harmonics (5d, 7f) were used instead of Cartesian components of the basis functions. All *ab initio* computations used the default frozen-core approximation, excluding the two core electrons of both C and O and the 10 core electrons of S from the MP2 and coupled-cluster correlation procedures. The DFT computations used a pruned numerical integration grid with 99 radial shells and 590 angular points per shell for all optimizations. All DFT and MP2 computations were performed with the Gaussian16 software package.[83] Molpro 2018 was used for all of the single-point computations.

## 3. RESULTS

**3.1. Two-Ring Oligomers.** Relaxed torsional scans for each two-ring oligomer are presented in Figure 3 (relative energy, $\Delta E$, versus $\tau$ from 0 to 180° in 10° increments) for the MP2 method and three DFT methods (B3LYP, M06-2X, and $\omega$B97XD), along with PNO-LCCSD(T)-F12 single-point values obtained using MP2 geometries. The general form of two-ring oligomers ($n$ = 2, where $R_X$, $R_Z$ = H) is depicted in Figure 2, with $\tau$ = 0 and 180° scan endpoints shown. All methods utilized the VTZ basis set except for PNO-LCCSD(T)-F12, which utilized VTZ-F12. The electronic energy for $\tau$ = 180° has been used as the reference energy because it corresponds to the global minimum for two of the oligomers. To maintain a consistent definition of $\Delta E$, the energetic reference point is kept as $\tau$ = 180° for all oligomers in this study, even those with a nonplanar global minimum. Table 1 provides a closer look at the minima for each of the two-ring oligomers, reporting $\Delta E$ and $\tau$ values for fully optimized structures, along with $\Delta E$ values of select scan points from Figure 3. The $\tau$ = 180° scan point is still used as the energetic reference for fully optimized structures. All of the same methods presented in relaxed scans are included in Table 1, with the addition of two coupled-cluster methods: CCSD(T) and CCSD(T)-F12 which use the VTZ and VTZ-F12 basis sets, respectively. For the explicitly correlated methods CCSD(T)-F12 and PNO-LCCSD(T)-F12, the two *ansätze* (*a* and *b*) gave very similar results; their relative energies for each two-ring structure differing by no more than 0.02 kcal mol$^{-1}$. Given that the results are so close, only the results obtained using an approximation are presented here, while the results for the other approximation can be found in the Supporting Information.

All of the two-ring oligomers have two minima at or near $\tau$ = 0 and 180° (sometimes referred to as *syn* and *anti* conformations, respectively). Fn−Fn (Figure 3 and top of Table 1) has a planar global minimum (GM) with $\tau$ = 180° for all methods. The results vary somewhat for the local minimum (LM) near $\tau$ = 0°. As seen in the first column of data in Table 3, the fully optimized LM is planar for all three DFT methods, but the MP2 optimization leads to a nonplanar structure with $\tau$ = 18.1°. This matches with the previously reported value of 16.3°,[57] which was also obtained using MP2-optimized geometries. All of the coupled-cluster results reported in Table 1 not only confirm the nonplanar character predicted by the MP2 computations but also demonstrate the extremely flat nature of the potential energy surface within 20 or 30° of $\tau$ = 0°. Of all of the two-ring oligomers, Fn−Fn exhibits the largest energy difference between its two minima, with all coupled-


https://doi.org/10.1021/acs.jpca.1c04714
J. Phys. Chem. A XXXX, XXX, XXX−XXX

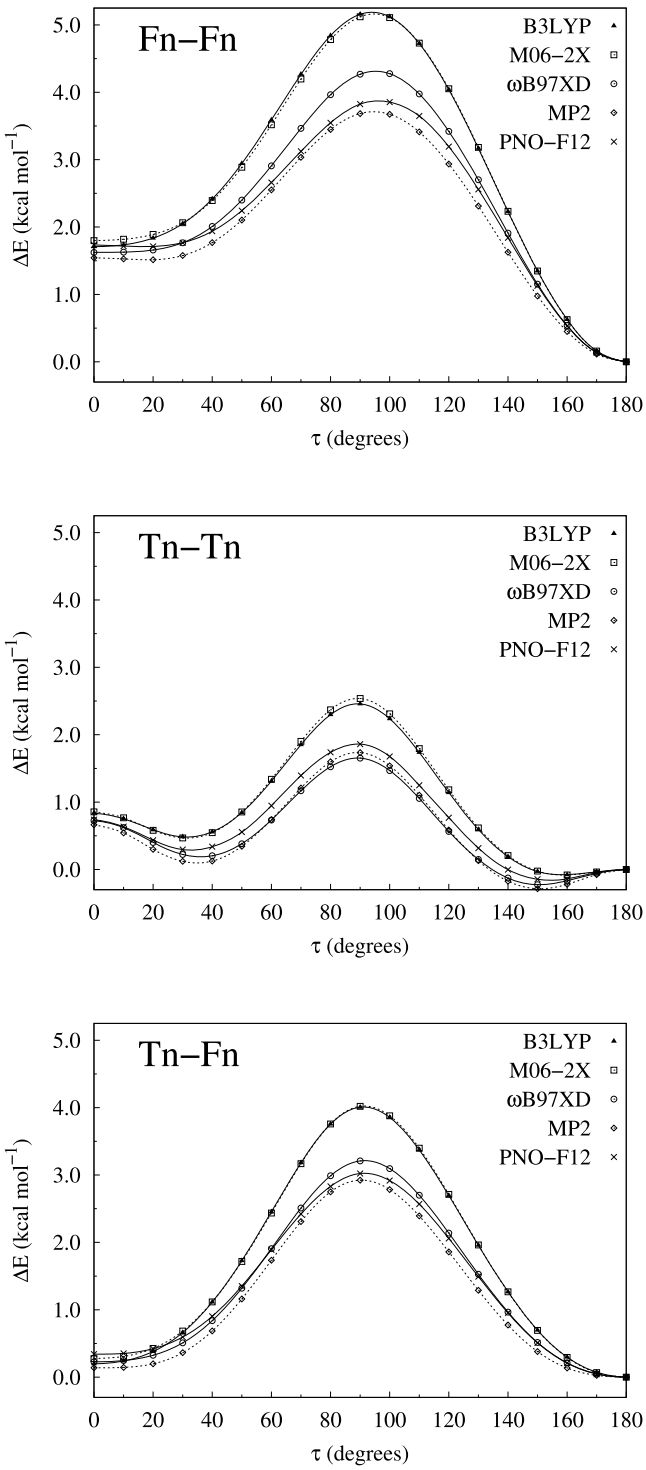


**Figure 3.** Relaxed scans of $\tau$ for two-ring systems with different methods. All methods used the VTZ basis set with the exception of PNO-LCCSD(T)-F12/VTZ-F12 (denoted PNO-F12). PNO-LCCSD(T)-F12 results were obtained using MP2/VTZ relaxed scan structures.

cluster electronic energies of the LM at $\tau = 0°$ being 1.7 kcal mol$^{-1}$ higher in energy than the GM at $\tau = 180°$.

In Figure 3, the energetic maximum of each relaxed scan corresponding to the rotational transition state, TS, occurs near $\tau = 90°$. More specifically, fully optimized TS structures for each oligomer (energies and coordinates given in the Supporting Information) have torsional angles ranging from 89 to 96° and relative energies that deviate by no more than 0.04 kcal mol$^{-1}$ from the $\Delta E$ values tabulated in Table 1 for $\tau$ constrained to 90°. Therefore, $\Delta E$ at $\tau = 90°$ is used to estimate the rotational barrier height of these two-ring structures as well as the larger three- and four-ring oligomers. Using $\Delta E$ at $\tau = 90°$ from Table 1, Fn−Fn has an electronic rotational barrier of approximately 3.9 kcal mol$^{-1}$ based on the coupled-cluster results. This closely matches the previously reported barrier height of 4.0 kcal mol$^{-1}$ that was obtained from focal-point analyses.[57]

The other two-ring systems, Tn−Tn and Tn−Fn, are analyzed in a similar manner. For Tn−Tn (Figure 3 and middle of Table 1), neither the GM nor the LM is planar, which leads to some negative $\Delta E$ values near $\tau = 150°$. Both the local and global optimized Tn−Tn minima are twisted out of plane by about 30°, as indicated by the corresponding angles in the first two columns of data in Table 1. The energy barrier to planarity is approximately 0.2 kcal mol$^{-1}$ for the *anti* minimum and approximately 0.5 kcal mol$^{-1}$ for the *syn* minimum at the coupled-cluster level of theory. The previously referenced computational study reports $\tau$ values of 32.3 and 156.3° for the LM and GM, respectively, and nearly identical barriers to planarity as those mentioned above.[57] The corresponding experimental values of $\tau$ (obtained via gas-phase electron diffraction) are 36 ± 5° and 148 ± 3°.[39] For the $\omega$B97XD and MP2 methods in conjunction with the VTZ basis set, torsional angles for both fully optimized minima fall within the confidence intervals of the experimental values. The coupled-cluster energy differences between the two Tn−Tn minima are approximately 0.4 kcal mol$^{-1}$, much smaller than the 1.7 kcal mol$^{-1}$ difference for the Fn−Fn minima. Tn−Tn has the smallest coupled-cluster rotational barrier of the two-ring systems, at or just below 2 kcal mol$^{-1}$, which is consistent with the previously reported value of 2.2 kcal mol$^{-1}$.[57]

The GM and LM of Tn−Fn (Figure 3 and bottom of Table 1) are both planar. Interestingly, the two minima for this heterogeneous system are essentially isoenergetic, whereas the global minima (with $\tau$ at or near 180°) have distinctly lower energies than the corresponding local minima (with $\tau$ at or near 0°) for the homogeneous Fn−Fn and Tn−Tn systems. The coupled-cluster results for Tn−Fn indicate that the GM and LM differ in energy by no more than 0.3 kcal mol$^{-1}$ and that they are separated by a rotational barrier of approximately 3.1 kcal mol$^{-1}$, both of which are identical to previously reported values.[55]

The CCSD(T)-F12 computations were performed with an additional basis set (VQZ-F12) to provide benchmark energetics near the CCSD(T) complete basis set limit. These $\Delta E$ values have been relegated to the Supporting Information because they are virtually identical to the corresponding CCSD(T)-F12 data presented in Table 3 that were obtained with the smaller VTZ-F12 basis set. The triple- and quadruple-$\zeta$ CCSD(T)-F12 results never differ by more than 0.1 kcal mol$^{-1}$, and typically by only a few hundredths of a kcal mol$^{-1}$ near the minima. The equivalent deviations associated with the CCSD(T)/VTZ relative energies tend to be slightly larger but still ≤0.3 kcal mol$^{-1}$. Even the PNO-LCCSD(T)-F12/VTZ-F12 $\Delta E$ data in Table 3 fall within 0.1 kcal mol$^{-1}$ of the corresponding CCSD(T)-F12/VQZ-F12 benchmark values. Consequently, the computationally efficient PNO-LCCSD(T)-F12 method and VTZ-F12 basis set were selected for the extension of this energetic analysis to the three- and four-ring systems.


https://doi.org/10.1021/acs.jpca.1c04714
J. Phys. Chem. A XXXX, XXX, XXX−XXX

**Table 1. Torsional Angles ($\tau$ in Degrees) of the Optimized Local and Global Minima (LM and GM, Respectively) for Two-Ring Systems, along with Their Relative Electronic Energies ($\Delta E$ in kcal mol$^{-1}$, Referenced to the $\tau$ = 180° Structure) and $\Delta E$ of Three Partially Optimized Structures (with $\tau$ Fixed at 0, 90, and 180°)**

| method | $\tau$ | | ΔE | | | | |
|---|---|---|---|---|---|---|---|
| | LM | GM | 0° | LM[a] | 90° | GM[a] | 180° |
| | | | Fn−Fn | | | | |
| B3LYP | 0.0 | 180.0 | +1.71 | [+1.71] | +5.16 | [0.00] | 0.00 |
| M06-2X | 0.0 | 180.0 | +1.80 | [+1.80] | +5.12 | [0.00] | 0.00 |
| ωB97XD | 0.0 | 180.0 | +1.62 | [+1.62] | +4.27 | [0.00] | 0.00 |
| MP2 | 18.1 | 180.0 | +1.54 | +1.51 | +3.68 | [0.00] | 0.00 |
| CCSD(T)[b] | | | +1.79 | +1.74 | +3.93 | [0.00] | 0.00 |
| PNO-LCCSD(T)-F12[b] | | | +1.74 | +1.71 | +3.82 | [0.00] | 0.00 |
| CCSD(T)-F12[b] | | | +1.73 | +1.71 | +3.91 | [0.00] | 0.00 |
| | | | Tn−Tn | | | | |
| B3LYP | 31.5 | 158.6 | +0.84 | +0.48 | +2.46 | −0.08 | 0.00 |
| M06-2X | 31.3 | 158.9 | +0.86 | +0.47 | +2.54 | −0.08 | 0.00 |
| ωB97XD | 36.1 | 150.6 | +0.73 | +0.19 | +1.65 | −0.23 | 0.00 |
| MP2 | 34.9 | 150.8 | +0.66 | +0.10 | +1.73 | −0.28 | 0.00 |
| CCSD(T)[b] | | | +0.86 | +0.30 | +1.75 | −0.19 | 0.00 |
| PNO-LCCSD(T)-F12[b] | | | +0.74 | +0.29 | +1.86 | −0.15 | 0.00 |
| CCSD(T)-F12[b] | | | +0.76 | +0.29 | +1.95 | −0.15 | 0.00 |
| | | | Tn−Fn | | | | |
| B3LYP | 0.0 | 180.0 | +0.20 | [+0.20] | +4.01 | [0.00] | 0.00 |
| M06-2X | 0.0 | 180.0 | +0.28 | [+0.28] | +4.02 | [0.00] | 0.00 |
| ωB97XD | 0.0 | 180.0 | +0.23 | [+0.23] | +3.21 | [0.00] | 0.00 |
| MP2 | 0.0 | 180.0 | +0.14 | [+0.14] | +2.92 | [0.00] | 0.00 |
| CCSD(T)[b] | | | +0.31 | [+0.31] | +3.05 | [0.00] | 0.00 |
| PNO-LCCSD(T)-F12[b] | | | +0.34 | [+0.34] | +3.02 | [0.00] | 0.00 |
| CCSD(T)-F12[b] | | | +0.31 | [+0.31] | +3.10 | [0.00] | 0.00 |

[a]Square brackets indicate that a fully optimized structure is planar with $\tau$ = 0 or 180°. [b]Single-point energies computed with MP2/VTZ geometries.

The benchmark coupled-cluster data in Figure 3, Table 1, and the Supporting Information can be used to help gauge the performance of some less demanding methods for the torsional energetics of oligomers. The ωB97XD and MP2 methods give $\Delta E$ values close to the coupled-cluster reference values, with maximum deviations falling between 0.2 and 0.4 kcal mol$^{-1}$ for all three systems. With torsional profiles that closely match those from coupled-cluster computations, the ωB97XD method was selected to characterize the larger oligomers ($n$ = 3 and 4).

**3.2. Three-Ring Oligomers.** The same torsional profiles about $\tau$ are examined for the three-ring systems. As depicted in Figure 2, the $R_X$ substituent changes from H to either Fn or Tn in the progression to $n$ = 3 from $n$ = 2. This additional ring will be prepended to the labels used for the two-ring systems and will include a subscript 0 or 180° to indicate the value of the fixed torsional angle between the $R_X$ heteroatom and X about the corresponding carbon−carbon bond between the rings (e.g., $Fn_0$ Fn−Fn). The relative PNO-LCCSD(T)-F12/VTZ-F12 electronic energies are plotted in Figure 4 for these systems ($R_Z$ = H and $R_X$ = Fn or Tn) using the structures obtained from ωB97XD/VTZ relaxed scans from $\tau$ = 0 to 180°. The results for the corresponding two-ring systems ($R_X$, $R_Z$ = H) utilizing the same levels of theory are included for comparison. The $\Delta E$ values for the $\tau$ = 0, 90, and 180° scan points are collected in Table 2. The corresponding CCSD(T)/VTZ and CCSD(T)-F12/VTZ-F12 data are tabulated in the Supporting Information, and relative energies obtained from these two different coupled-cluster procedures deviated by no more than 0.1 kcal mol$^{-1}$ from any of the corresponding values reported in Table 2.

The scans of these three-ring systems presented in Figure 4 demonstrate that the addition of another ring to Fn−Fn, Tn−Tn, or Tn−Fn at the $R_X$ position (Figure 2) has little effect on the torsional profile. For example, the two minima on each curve for the $R_X$Tn−Tn systems occur near $\tau$ = 30 and 150° regardless of the identity (H, Fn, or Tn) or orientation ($\tau_X$ = 0 or 180°) of $R_X$. The electronic energies for the lowest point on each curve near $\tau$ = 30° consistently lie 0.5 ± 0.1 kcal mol$^{-1}$ above those at the bottom of the well near 150°. Similarly, the minima on the torsional curves for the $R_X$Fn−Fn, $R_X$Tn−Fn, and $R_X$Fn−Tn systems are located at or near 0 or 180° for all permutations of $R_X$. The differences in the electronic energy between those lowest points are 1.7 ± 0.2 kcal mol$^{-1}$ for $R_X$Fn−Fn and 0.3 ± 0.1 kcal mol$^{-1}$ for $R_X$Tn−Fn and $R_X$Fn−Tn. The rotational barrier heights also display very minor variations as $R_X$ changes. For $R_X$Tn−Tn, barriers to rotation fall within a small range of 2.0−2.3 kcal mol$^{-1}$. The range of energy barriers for the remaining oligomers are 3.8−4.2 kcal mol$^{-1}$ for $R_X$Fn−Fn and 3.0−3.4 kcal mol$^{-1}$ for heterogeneous oligomers ($R_X$Tn−Fn and $R_X$Fn−Tn).

Considering all of the plots as a whole, it becomes evident that when $R_X$ is attached to a thiophene ring, as in $R_X$Tn−Tn and $R_X$Tn−Fn, the identity and orientation of the additional $R_X$ ring has essentially no effect on the resulting torsional profile. For oligomers where $R_X$ is attached to a furan ring ($R_X$Fn−Fn and $R_X$Fn−Tn), variations in the torsional profile upon changing $R_X$ only become larger than 0.1 kcal mol$^{-1}$ for substituents with a $\tau_X$ value of 0°, such as $Fn_0$ Fn−Fn and $Tn_0$ Fn−Tn. Overall, the extension of an oligomer via the addition of a furan or thiophene ring results in only very minor changes to an oligomer's torsional profile when moving from a two-ring


https://doi.org/10.1021/acs.jpca.1c04714
J. Phys. Chem. A XXXX, XXX, XXX−XXX

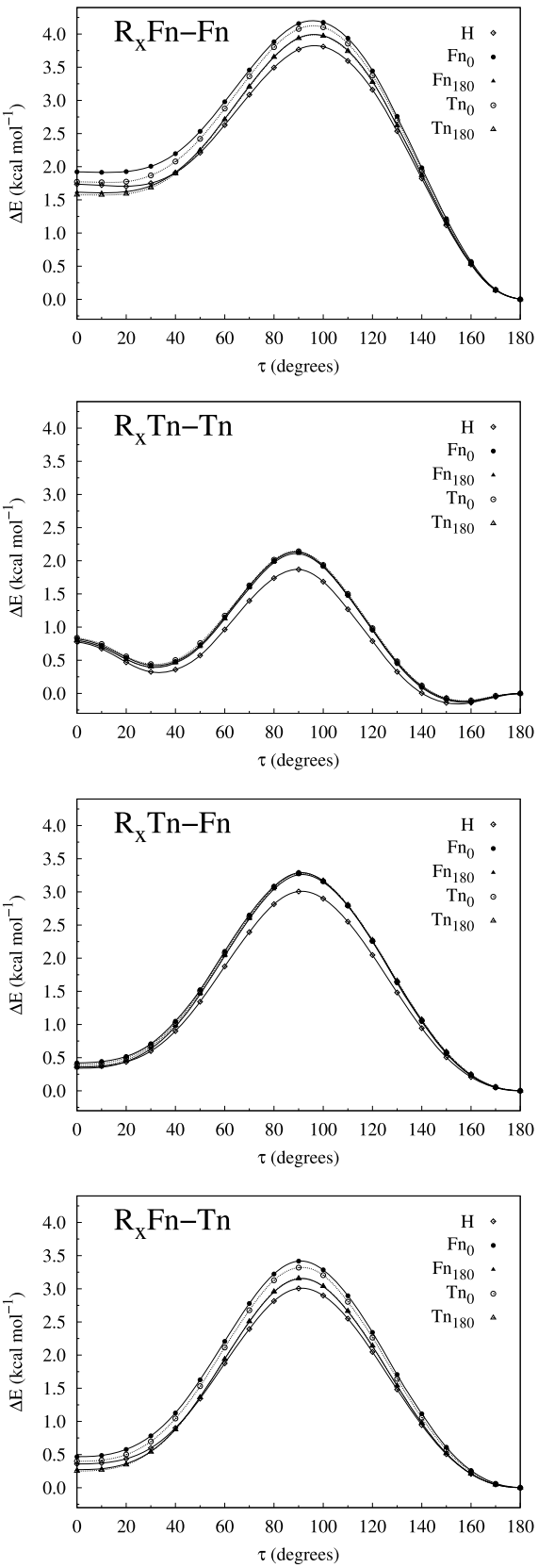


**Figure 4.** Relaxed scans of $\tau$ for three-ring oligomers with their two-ring counterparts included for reference, all at the PNO-LCCSD(T)-F12/VTZ-F12 level of theory on $\omega$B97XD/VTZ relaxed scan structures. The identity and orientation ($\tau_X$ value) of $R_X$ is indicated in the legend.

**Table 2. Relative Energies ($\Delta E$ in kcal mol$^{-1}$) for the $\tau$ = 0, 90, and 180° Relaxed Scan Points of All Three-Ring Oligomers at the PNO-LCCSD(T)-F12/VTZ-F12 Level of Theory on $\omega$B97XD/VTZ Geometries**

| | $\Delta E$ | | |
|---|---|---|---|
| $R_X$ | 0° | 90° | 180° |
| | $R_X$Fn−Fn | | |
| $Fn_0$ | 1.92 | 4.16 | 0.00 |
| $Fn_{180}$ | 1.62 | 3.94 | 0.00 |
| $Tn_0$ | 1.77 | 4.08 | 0.00 |
| $Tn_{180}$ | 1.58 | 3.94 | 0.00 |
| | $R_X$Tn−Tn | | |
| $Fn_0$ | 0.82 | 2.13 | 0.00 |
| $Fn_{180}$ | 0.80 | 2.11 | 0.00 |
| $Tn_0$ | 0.84 | 2.14 | 0.00 |
| $Tn_{180}$ | 0.80 | 2.13 | 0.00 |
| | $R_X$Tn−Fn | | |
| $Fn_0$ | 0.42 | 3.29 | 0.00 |
| $Fn_{180}$ | 0.34 | 3.26 | 0.00 |
| $Tn_0$ | 0.40 | 3.28 | 0.00 |
| $Tn_{180}$ | 0.37 | 3.28 | 0.00 |
| | $R_X$Fn−Tn | | |
| $Fn_0$ | 0.47 | 3.42 | 0.00 |
| $Fn_{180}$ | 0.27 | 3.15 | 0.00 |
| $Tn_0$ | 0.40 | 3.32 | 0.00 |
| $Tn_{180}$ | 0.25 | 3.16 | 0.00 |

to a three-ring system, and the identity and orientation of the additional ring has little effect on the resulting profile.

**3.3. Four-Ring Oligomers.** Analogous torsional profiles are examined for the four-ring oligomers, focusing on the relative energies associated with $\tau$ = 0, 90, and 180°. For these oligomers, both $R_X$ and $R_Z$ change from H to either Fn or Tn (in the progression from $n$ = 2 to 4 in Figure 2). The notation used for these oligomers prepends $R_X$ and appends $R_Z$ to the labels used for the two-ring systems (e.g., $R_X$Fn−Fn $R_Z$). As with the three-ring oligomers, $\tau_X$ and $\tau_Z$ values (fixed at either 0 or 180°) are indicated as subscripts to $R_X$ and $R_Z$. Relative energies for each four-ring oligomer are presented in Table 3, where each row corresponds to a different oligomer with the $R_X$ and $R_Z$ substituents indicated in the first two columns. Note that results are only reported for unique permutations of the $R_X$Fn−Fn $R_Z$ and $R_X$Tn−Tn $R_Z$ systems (top and middle of Table 3) because some arrangements are equivalent (such as $Fn_0$ Fn−Fn $Fn_{180}$ and $Fn_{180}$ Fn−Fn $Fn_0$). In addition, CCSD(T)/VTZ single-point computations were performed on the same $\omega$B97XD optimized geometries of the $\tau$ = 0, 90, and 180° relaxed scan points for all four-ring oligomers. Their relative energies are tabulated in the Supporting Information. The relative energies obtained using CCSD(T) differed by no more than 0.2 kcal mol$^{-1}$ from any of the data points reported in Table 3.

The addition of a fourth furan or thiophene ring at the $R_Z$ position (Figure 2) has very little effect on the resulting torsional profile, and the changes that do occur closely mirror those for the corresponding addition of the third ring at $R_X$. The configurations with $\tau$ constrained to 180° consistently have the lowest electronic energies for all of the four-ring oligomers. For configurations where $\tau$ = 0°, the PNO-LCCSD(T)-F12/VTZ-F12 energy increases from 180° scan points by approximately 1.4−2.1 kcal mol$^{-1}$ for $R_X$Fn−Fn $R_Z$ systems, 0.8−0.9 kcal mol$^{-1}$ for $R_X$Tn−Tn $R_Z$ systems, and


https://doi.org/10.1021/acs.jpca.1c04714
J. Phys. Chem. A XXXX, XXX, XXX−XXX

**Table 3. Relative Energies ($\Delta E$ in kcal mol$^{-1}$) for $\tau$ = 0, 90, and 180° Scan Points at the PNO-LCCSD(T)-F12/VTZ-F12 Level of Theory on $\omega$B97XD/VTZ Geometries for All Four-Ring Oligomers**

| substituents | | ΔE | | |
|---|---|---|---|---|
| $R_X$ | $R_Z$ | 0° | 90° | 180° |
| | | $R_X$Fn−Fn$R_Z$ | | |
| $Fn_0$ | $Fn_0$ | 2.14 | 4.59 | 0.00 |
| $Fn_0$ | $Fn_{180}$ | 1.70 | 4.34 | 0.00 |
| $Fn_{180}$ | $Fn_{180}$ | 1.49 | 4.11 | 0.00 |
| $Tn_0$ | $Tn_0$ | 1.71 | 4.41 | 0.00 |
| $Tn_0$ | $Tn_{180}$ | 1.49 | 4.26 | 0.00 |
| $Tn_{180}$ | $Tn_{180}$ | 1.40 | 4.12 | 0.00 |
| $Fn_0$ | $Tn_0$ | 1.92 | 4.49 | 0.00 |
| $Fn_0$ | $Tn_{180}$ | 1.64 | 4.34 | 0.00 |
| $Fn_{180}$ | $Tn_0$ | 1.53 | 4.24 | 0.00 |
| $Fn_{180}$ | $Tn_{180}$ | 1.45 | 4.11 | 0.00 |
| | | $R_X$Tn−Tn$R_Z$ | | |
| $Fn_0$ | $Fn_0$ | 0.89 | 2.43 | 0.00 |
| $Fn_0$ | $Fn_{180}$ | 0.84 | 2.40 | 0.00 |
| $Fn_{180}$ | $Fn_{180}$ | 0.82 | 2.38 | 0.00 |
| $Tn_0$ | $Tn_0$ | 0.89 | 2.45 | 0.00 |
| $Tn_0$ | $Tn_{180}$ | 0.84 | 2.43 | 0.00 |
| $Tn_{180}$ | $Tn_{180}$ | 0.81 | 2.41 | 0.00 |
| $Fn_0$ | $Tn_0$ | 0.89 | 2.44 | 0.00 |
| $Fn_0$ | $Tn_{180}$ | 0.83 | 2.42 | 0.00 |
| $Fn_{180}$ | $Tn_0$ | 0.84 | 2.41 | 0.00 |
| $Fn_{180}$ | $Tn_{180}$ | 0.82 | 2.40 | 0.00 |
| | | $R_X$Tn−Fn$R_Z$ | | |
| $Fn_0$ | $Fn_0$ | 0.55 | 3.74 | 0.00 |
| $Fn_{180}$ | $Fn_0$ | 0.42 | 3.68 | 0.00 |
| $Tn_0$ | $Fn_0$ | 0.51 | 3.73 | 0.00 |
| $Tn_{180}$ | $Fn_0$ | 0.44 | 3.72 | 0.00 |
| $Fn_0$ | $Tn_0$ | 0.45 | 3.63 | 0.00 |
| $Fn_{180}$ | $Tn_0$ | 0.34 | 3.57 | 0.00 |
| $Tn_0$ | $Tn_0$ | 0.41 | 3.62 | 0.00 |
| $Tn_{180}$ | $Tn_0$ | 0.36 | 3.61 | 0.00 |
| $Fn_0$ | $Fn_{180}$ | 0.30 | 3.45 | 0.00 |
| $Fn_{180}$ | $Fn_{180}$ | 0.26 | 3.42 | 0.00 |
| $Tn_0$ | $Fn_{180}$ | 0.27 | 3.43 | 0.00 |
| $Tn_{180}$ | $Fn_{180}$ | 0.28 | 3.44 | 0.00 |
| $Fn_0$ | $Tn_{180}$ | 0.28 | 3.46 | 0.00 |
| $Fn_{180}$ | $Tn_{180}$ | 0.24 | 3.42 | 0.00 |
| $Tn_0$ | $Tn_{180}$ | 0.24 | 3.44 | 0.00 |
| $Tn_{180}$ | $Tn_{180}$ | 0.24 | 3.46 | 0.00 |

0.2−0.6 kcal mol$^{-1}$ for heterogeneous $R_X$Tn−Fn $R_Z$ systems (top, middle, and bottom of Table 3, respectively). These ranges of $\Delta E$ values fall within *ca.* 0.2 kcal mol$^{-1}$ of the corresponding values for $n$ = 3. Also, as was noted for the three-ring systems, the four-ring systems demonstrate that changing the identity of a substituent ($R_X$ or $R_Z$) attached to a thiophene ring has a smaller impact on the torsional profile than changing one attached to a furan ring.

The trends in the PNO-LCCSD(T)-F12/VTZ-F12 torsional barrier heights (estimated as $\Delta E$ at $\tau$ = 90°) for $n$ = 4 are also consistent with those for $n$ = 2 and 3. The largest barriers (≈ 4.3 kcal mol$^{-1}$) are encountered for rotation about the central bond between two Fn rings (i.e., $R_X$Fn−Fn $R_Z$), while the smallest barriers (≈2.4 kcal mol$^{-1}$) are associated with rotation about the bond between two Tn rings (i.e., $R_X$Tn−Tn $R_Z$). The barrier for rotation about the bond connecting Fn and Tn rings falls between the other two systems at ≈3.5 kcal mol$^{-1}$ for $R_X$Tn−Fn $R_Z$. For all of the different sets of oligomers, the barrier height consistently increases by approximately 0.3 kcal mol$^{-1}$ for each oligomer extension: two to three rings and three to four rings.

## 4. CONCLUSIONS

This work performs a systematic conformational analysis of 55 unique oligomers, composed of furan and thiophene units, related to common $\pi$-conjugated bridges for organic semiconductors. Three different DFT methods were used along with MP2 and three different coupled-cluster methods (CCSD(T), CCSD(T)-F12, and PNO-LCCSD(T)-F12) to study energetics and the torsional profiles of the aforementioned systems. Of the DFT methods tested for the two-ring systems, $\omega$B97XD proved to be the most reliable for reproducing MP2 and coupled-cluster torsional profiles. For all of the oligomers consisting of two heterocycles, PNO-LCCSD(T)-F12/VTZ-F12 relative energies differed by no more than 0.1 kcal mol$^{-1}$ from the corresponding CCSD(T)-F12 values computed with the VTZ-F12 and VQZ-F12 basis sets. For both the three- and four-ring systems, the PNO-LCCSD(T)-F12/VTZ-F12 relative energies of the $\tau$ = 0, 90, and 180° relaxed scan points differed by no more than 0.2 kcal mol$^{-1}$ from the corresponding CCSD(T)/VTZ relative energies. These benchmark results could be used to perform a more extensive calibration of other less demanding methods for the larger oligomers, but such a task is outside of the focus of this work.

Two fully optimized minima have been characterized for the systems with two rings. In each case, the global minimum has a torsional angle of/near 180° between the heteroatoms about the carbon−carbon bond connecting the two rings, whereas $\tau$ is equal to or close to 0° for the local minimum. In the homogeneous Fn−Fn system, the electronic energy of the planar global minimum is nearly 2 kcal mol$^{-1}$ lower than that of the quasi-planar local minimum near the CCSD(T) CBS limit, and they are separated by a rotational barrier on the order of 4 kcal mol$^{-1}$. These energy differences are significantly smaller for Tn−Tn, where the local and global minimum exhibit the largest deviations from planarity (*ca.* 30°) and the difference in energy between them decreases to 0.4 kcal mol$^{-1}$. The Tn−Tn rotational barrier is also reduced to 2 kcal mol$^{-1}$. Although the heterogeneous Tn−Fn oligomer also has a very small energy difference between its two minima (0.3 kcal mol$^{-1}$), both optimized structures are planar, and the rotational barrier height is just over 3 kcal mol$^{-1}$ (significantly larger than for Tn−Tn). The overall trend for the energy difference between the local and global minima is Tn−Fn $\lesssim$ Tn−Tn $\ll$ Fn−Fn, while the trend for the rotational barrier is Tn−Tn < Tn−Fn < Fn−Fn.

Increasing the length of the oligomer by changing $R_X$ and $R_Z$ from H to Tn and/or Fn does not lead to significant changes in the barrier heights or the relative energies of the *syn* and *anti* conformations near $\tau$ = 0 and 180°, respectively. Trends in the rotational barrier heights for the three- and four-ring oligomers remain the same as the two-ring oligomers: $R_X$Tn−Tn $R_Z$ < $R_X$Tn−Fn $R_Z$ < $R_X$Fn−Fn $R_Z$. The trend in energy differences between the $\tau$ = 0° and $\tau$ = 180° configurations (roughly similar to the energy difference between the minima) remains $R_X$Tn−Fn $R_Z$ $\lesssim$ $R_X$Tn−Tn $R_Z$ $\ll$ $R_X$Fn−Fn $R_Z$ for all oligomers ($n$ = 2, 3, and 4). Typically, the largest change in the conformational profiles when moving from a shorter to a


https://doi.org/10.1021/acs.jpca.1c04714
J. Phys. Chem. A XXXX, XXX, XXX−XXX

longer oligomer ($n$ = 2 to $n$ = 3 or 4) was in the rotational barrier height, estimated as $\Delta E$ at $\tau = 90°$, with the maximum change being 0.8 kcal mol$^{-1}$ at the PNO-LCCSD(T)-F12/VTZ-F12 level of theory (for the system where X and Z = O in Figure 2). The changes induced by extending the Tn and Fn ring systems tended to be even smaller near the minima ($\tau = 0$ and 180°). Taken altogether, these patterns illustrate that extending the oligomer using Tn and Fn rings has a very small effect on the overall torsional profile about the CC bond connecting the central Fn and/or Tn units.

## ■ ASSOCIATED CONTENT

### Supporting Information

The Supporting Information is available free of charge at https://pubs.acs.org/doi/10.1021/acs.jpca.1c04714.

Cartesian coordinates and additional energetic data (PDF)

## ■ AUTHOR INFORMATION


### Corresponding Author

**Gregory S. Tschumper** − *Department of Chemistry and Biochemistry, University of Mississippi, University, Mississippi 38677-1848, United States;* orcid.org/0000-0002-3933-2200; Email: tschumpr@olemiss.edu

### Authors

**Morgan A. Perkins** − *Department of Chemistry and Biochemistry, University of Mississippi, University, Mississippi 38677-1848, United States*

**Laura M. Cline** − *Department of Chemistry and Biochemistry, University of Mississippi, University, Mississippi 38677-1848, United States*

Complete contact information is available at: https://pubs.acs.org/10.1021/acs.jpca.1c04714


### Author Contributions

G.S.T. designed and supervised the project. L.M.C. and M.A.P. performed the DFT and MP2 computations. M.A.P. carried out all of the coupled-cluster work. All authors contributed to the analysis of the data and writing of the manuscript.

### Notes

The authors declare no competing financial interest.

## ■ ACKNOWLEDGMENTS

This work was supported in part by the National Science Foundation (CHE-166498). The Mississippi Center for Supercomputing Research (MCSR) is also thanked for a generous allocation of time on their computational resources.

## ■ REFERENCES


(1) Bradley, A.; Hammes, J. P. Electrical Properties of Thin Organic Films. *J. Electrochem. Soc.* **1963**, *110*, 15−22.

(2) Chiang, C. K.; Fincher, C. R.; Park, Y. W.; Heeger, A. J.; Shirakawa, H.; Louis, E. J.; Gau, S. C.; MacDiarmid, A. G. Electrical Conductivity in Doped Polyacetylene. *Phys. Rev. Lett.* **1977**, *39*, 1098−1101.

(3) Burroughes, J. H.; Bradley, D. D. C.; Brown, A. R.; Marks, R. N.; Mackay, K.; Friend, R. H.; Burns, P. L.; Holmes, A. B. Light-emitting diodes based on conjugated polymers. *Nature* **1990**, *347*, 539−541.

(4) Garnier, F. Thin film transistors based on organic conjugated semiconductors. *Curr. Opin. Solid State Mater. Sci.* **1997**, *2*, 455−461.

(5) Garnier, F. Organic-Based Eletronics *à la Carte*. *Acc. Chem. Res.* **1999**, *32*, 209−215.

(6) Harbeke, G.; Baeriswyl, D.; Kiess, H.; Kobel, W. Polarons and Bipolarons in Doped Polythiophenes. *Phys. Scr.* **1986**, *T13*, 302−305.

(7) Tsumura, A.; Koezuka, H.; Ando, T. Macromolecular electronic device: Field-effect transistor with a polythiophene thin film. *Appl. Phys. Lett.* **1986**, *49*, 1210−1212.

(8) Garnier, F.; Horowitz, G.; Peng, X.; Fichou, D. An all-organic "soft" thin film transistor with very high carrier mobility. *Adv. Mater.* **1990**, *2*, 592−594.

(9) Horowitz, G.; Peng, X.; Fichoi, D.; Garnier, F. The oligothiophene-based field-effect transistor: How it works and how to improve it. *J. Appl. Phys.* **1990**, *67*, 528−532.

(10) Rogers, J. A.; Bao, Z.; Baldwin, K.; Dodabalapur, A.; Crone, B.; Raju, V. R.; Kuck, V.; Katz, H.; Amundson, K.; Ewing, J.; et al. Paper-like electronic displays: Large-area rubber-stamped plastic sheets of electronics and microencapsulated electrophoretic inks. *Proc. Natl. Acad. Sci. U.S.A.* **2001**, *98*, 4835−4840.

(11) Karpe, S.; Cravino, A.; Frère, P.; Allain, M.; Mabon, G.; Roncali, J. 3D $\pi$-Conjugated Oligothiophenes Based on Sterically Twisted Bithiophene Nodes. *Adv. Funct. Mater.* **2007**, *17*, 1163−1171.

(12) Zaumseil, J.; Sirringhaus, H. Electron and Ambipolar Transport in Organic Field-Effect Transistors. *Chem. Rev.* **2007**, *107*, 1296−1323.

(13) Leitch, A. A.; Stobo, K. A.; Hussain, B.; Ghoussoub, M.; Ebrahimi-Takalloo, S.; Servati, P.; Korobkov, I.; Brusso, J. L. Oligothiophene-Functionalized Benzene and Tetrathienoanthracene: Effect of Enhanced $\pi$-Conjugation on Optoelectronic Properties, Self-Assembly and Device Performance. *Eur. J. Org. Chem.* **2013**, *2013*, 5854−5863.

(14) Borrelli, D. C.; Lee, S.; Gleason, K. K. Optoelectronic properties of polythiophene thin films and organic TFTs fabricated by oxidative chemical vapor deposition. *J. Mater. Chem. C* **2014**, *2*, 7223−7231.

(15) Ibrahim, S. R. M.; Abdallah, H. M.; El-Halawany, A.; Mohamed, G. A. Naturally occurring thiophenes: isolation, purification, structural elucidation, and evaluation of bioactivities. *Phytochem. Rev.* **2016**, *15*, 197−220.

(16) Vaidyanathan, S.; Dötz, F.; Katz, H. E.; Lawrentz, U.; Granstrom, J.; Reichmanis, E. Investigation of Solubility-Field Effect Mobility Orthogonality in Substituted Phenylene-Thiophene Co-oligomers. *Chem. Mater.* **2007**, *19*, 4676−4681.

(17) Rasmussen, S. C.; Evenson, S. J.; McCausland, C. B. Fluorescent thiophene-based materials and their outlook for emissive applications. *Chem. Commun.* **2015**, *51*, 4528−4543.

(18) Ferraris, J. P.; Skiles, G. D. 'Substitutional alloys' of organic polymeric conductors. *Polymer* **1987**, *28*, 179−182.

(19) Joshi, M. V.; Hemler, C.; Cava, M. P.; Cain, J. L.; Bakker, M. G.; McKinley, A. J.; Metzger, R. M. Synthesis, electrical conductivity and electron paramagnetic resonance spectroscopy of polymers derived from NOPF6-doped XYZ-triheterocycles based on pyrrole, furan and thiophene. *J. Chem. Soc., Perkin Trans. 2* **1993**, *2*, 1081−1086.

(20) Parakka, J. P.; Cava, M. P. Furan- and pyrrole-containing analogs of $\alpha$-quinquethiophene: spectroscopic and electrochemical properties. *Synth. Met.* **1995**, *68*, 275−279.

(21) Huang, J.-D.; Wen, S.-H.; Deng, W.-Q.; Han, K.-L. Simulation of Hole Mobility in $\alpha$-Oligofuran Crystals. *J. Phys. Chem. B* **2011**, *115*, 2140−2147.

(22) Mitsui, C.; Soeda, J.; Miwa, K.; Tsuji, H.; Takeya, J.; Nakamura, E. Naphtho[2,1-b:6,5-b′]difuran: A Versatile Motif Available for Solution-Processed Single-Crystal Organic Field-Effect Transistors with High Hole Mobility. *J. Am. Chem. Soc.* **2012**, *134*, 5448−5451.

(23) Gidron, O.; Diskin-Posner, Y.; Bendikov, M. $\alpha$-Oligofurans. *J. Am. Chem. Soc.* **2010**, *132*, 2148−2150.

(24) Gidron, O.; Dadvand, A.; Sun, E. W.-H.; Chung, I.; Shimon, L. J. W.; Bendikov, M.; Perepichka, D. F. Oligofuran-containing molecules for organic electronics. *J. Mater. Chem. C* **2013**, *1*, 4358−4367.

(25) Binder, J. B.; Raines, R. T. Simple Chemical Transformation of Lignocellulosic Biomass into Furans for Fuels and Chemicals. *J. Am. Chem. Soc.* **2009**, *131*, 1979−1985.

(26) Diaz-Quijada, G. A.; Weinberg, N.; Holdcroft, S.; Pinto, B. M. Investigation of Barriers To Conformational Interchange in Oligothiophenes and Oligo(Thienyl)furans. *J. Phys. Chem. A* **2002**, *106*, 1266−1276.

(27) Miyata, Y.; Nishinaga, T.; Komatsu, K. Synthesis and Structural, Electronic, and Optical Properties of Oligo(thienylfurans)s in Comparison with Oligothiophenes and Oligofurans. *J. Org. Chem* **2005**, *70*, 1147−1153.

(28) Parra, R. D.; Hill, B. Conformational analysis of n-fluorine, 2,2′-X (n = 3 or 3′; X = bifuran, bithiophene, or thienylfuran): Ab initio, density functional, and multi-coefficient correlation results. *J. Mol. Struct.: THEOCHEM* **2010**, *940*, 61−69.

(29) Henssler, J. T.; Matzger, A. J. Regiochemical Effects of Furan Substitution on the Electronic Properties and Solid-State Structure of Partial Fused-Ring Oligothiophenes. *J. Org. Chem.* **2012**, *77*, 9298−9303.

(30) Jeffries-EL, M.; Kobilka, B. M.; Hale, B. J. Optimizing the Performance of Conjugated Polymers in Organic Photovoltaic Cells by Traversing Group 16. *Macromolecules* **2014**, *47*, 7253−7271.

(31) Zade, S. S.; Bendikov, M. From Oligomers to Polymer: Convergence in the HOMO-LUMO Gaps of Conjugated Oligomers. *Org. Lett.* **2006**, *8*, 5243−5246.

(32) Camarada, M. B.; Jaque, P.; Díaz, F. R.; del Valle, M. A. Oxidation potential of thiophene oligomers: Theoretical and experimental approach. *J. Polym. Sci., Part B: Polym. Phys.* **2011**, *49*, 1723−1733.

(33) Zade, S. S.; Zamoshchik, N.; Bendikov, M. From Short Conjugated Oligomers to Conjugated Polymers. Lessons from Studies on Long Conjugated Oligomers. *Acc. Chem. Res.* **2011**, *44*, 14−24.

(34) Sharma, S.; Bendikov, M. α-Oligofurans: A Computational Study. *Chem. − Eur. J.* **2013**, *19*, 13127−13139.

(35) Tortorella, S.; Talamo, M. M.; Cardone, A.; Pastore, M.; De Angelis, F. Benchmarking DFT and semi-empirical methods for a reliable and cost-efficient computational screening of benzofulvene derivatives as donor materials for small-molecule organic solar cells. *J. Phys.: Condens. Matter* **2016**, *28*, 074005.

(36) Sahu, H.; Shukla, R.; Goswami, J.; Gaur, P.; Panda, A. N. Alternating phenylene and furan/pyrrole/thiophene units-based oligomers: A computational study of the structures and optoelectronic properties. *Chem. Phys. Lett.* **2018**, *692*, 152−159.

(37) Steen, A. E.; Ellington, T. L.; Nguyen, S. T.; Balasubramaniam, S.; Chandrasiri, I.; Delcamp, J. H.; Tschumper, G. S.; Hammer, N. I.; Watkins, D. L. Characterization of Furan- and Thiophene-Containing Bispyridyl Oligomers via Spectroscopic, Electrochemical, and TD-DFT Methods. *J. Phys. Chem. C* **2019**, *123*, 15176−15185.

(38) Ortí, E.; Sánchez-Marín, J.; Merchán, M.; Tomás, F. Theoretical approach to the molecular conformation of nonfused biheterocycles. Bifurans and furylpyrroles. *J. Phys. Chem. A* **1987**, *91*, 545−551.

(39) Samdal, S.; Samuelsen, E. J.; Volden, H. V. Molecular conformation of 2,2′-bithiophene determined by gas phase electron diffraction and ab initio calculations. *Synth. Met.* **1993**, *59*, 259−265.

(40) Hernandez, V.; Lopez Navarrete, J. T. Ab initio study of torsional potentials in 2,2′-bithiophene and 3,4′- and 3,3′-dimethyl-2,2′-bithiophene as models of the backbone flexibility in poly-thiophene and poly(3-methylthiophene). *J. Chem. Phys.* **1994**, *101*, 1369−1377.

(41) Ortí, E.; Viruela, P. M.; Sánchez-Marín, J.; Tomás, F. Ab Initio Determination of the Geometric Structure and Internal Rotation Potential of 2,2'-Bithiophene. *J. Phys. Chem. A* **1995**, *99*, 4955−4963.

(42) Ciofalo, M.; Manna, G. L. Ab initio conformational study of 2,2′:5′,2″-terthiophene. *Chem. Phys. Lett.* **1996**, *263*, 73−78.

(43) Karpfen, A.; Choi, C. H.; Kertesz, M. Single-Bond Torsional Potentials in Conjugated Systems: A Comparison of ab Initio and Density Functional Results. *J. Phys. Chem. A* **1997**, *101*, 7426−7433.

(44) Alemán, C.; Domingo, V. M.; Fajarí, L.; Juliá, L.; Karpfen, A. Molecular and Electronic Structures of Heteroaromatic Oligomers: Model Compounds of Polymers with Quantum-Well Structures. *J. Org. Chem.* **1998**, *63*, 1041−1048.

(45) Viruela, P. M.; Viruela, R.; Ortí, E. Difficulties of density functional theory in predicting the torsional potential of 2,2′-bithiophene. *Int. J. Quantum Chem.* **1998**, *70*, 303−312.

(46) Millefiori, S.; Alparone, A.; Millefiori, A. Conformational properties of thiophene oligomers. *J. Heterocycl. Chem.* **2000**, *37*, 847−853.

(47) Duarte, H. A.; Santos, H. F. D.; Rocha, W. R.; De Almeida, W. B. Improved quantum mechanical study of the potential energy surface for the bithiophene molecule. *J. Chem. Phys.* **2000**, *113*, 4206−4215.

(48) Balbás, A.; González Tejera, M.; Tortajada, J. Influence of the electron correlation on computed properties of furan oligomers. *J. Mol. Struct.: THEOCHEM* **2001**, *572*, 141−150.

(49) Duarte, H. A.; Duani, H.; De Almeida, W. B. Ab initio correlated comparative study of the torsional potentials for 2,2′-bipyrrole and 2,2′-bifuran five membered heterocyclic dimers. *Chem. Phys. Lett.* **2003**, *369*, 114−124.

(50) Raos, G.; Famulari, A.; Marcon, V. Computational reinvestigation of the bithiophene torsion potential. *Chem. Phys. Lett.* **2003**, *379*, 364−372.

(51) Liu, F.; Zuo, P.; Meng, L.; Zheng, S. Configuration interaction study on the conformational and optical properties of excited furan oligomers. *J. Mol. Struct.: THEOCHEM* **2005**, *726*, 189−196.

(52) Liu, F.; Zuo, P.; Meng, L.; Zheng, S. J. On the optical properties of thiophene oligomers: configuration interaction study on their ground (S0) and first singlet excited (S1) states. *J. Mol. Struct.: THEOCHEM* **2005**, *726*, 161−169.

(53) Sancho-García, J. C.; Karpfen, A. Conformational Analysis of 2,2′-bifuran: Correlated High-level Ab initio and DFT Results. *Theor. Chem. Acc.* **2006**, *115*, 427−433.

(54) Sancho-García, J. C.; Karpfen, A. Conformational Analysis of 2,2′-bifuran: Correlated High-level Ab initio and DFT Results. *Theor. Chem. Acc.* **2006**, *115*, 427−433.

(55) Sancho-García, J. C.; Karpfen, A. Theoretical approach to the conformational analysis of heteroaromatic dimers: 2-(2-Thienyl)-pyrrole, 2-(2-thienyl)furan, and 2-(2-furyl)pyrrole. *Chem. Phys. Lett.* **2009**, *473*, 49−56.

(56) Sánchez-Sanz, G.; Alkorta, I.; Elguero, J. A theoretical study of the conformation of 2,2′-bifuran, 2,2′-bithiophene, 2,2′-bitelluro-phene and mixed derivatives: Chalcogen-chalcogen interactions or dipole-dipole effects? *Comput. Theor. Chem.* **2011**, *974*, 37−42.

(57) Bloom, J. W. G.; Wheeler, S. E. Benchmark Torsional Potentials of Building Blocks for Conjugated Materials: Bifuran, Bithiophene, and Biselenophene. *J. Chem. Theory Comput.* **2014**, *10*, 3647−3655.

(58) Guskova, O. A. On the Inter-Ring Torsion Potential of 2,2′-Bithiophene: A Review of Open Problems and Current Proposals. In *Quantum Systems in Physics, Chemistry, and Biology*; Springer, 2017; pp 209−230.

(59) Lin, J. B.; Jin, Y.; Lopez, S. A.; Druckerman, N.; Wheeler, S. E.; Houk, K. N. Torsional Barriers to Rotation and Planarization in Heterocyclic Oligomers of Value in Organic Electronics. *J. Chem. Theory Comput.* **2017**, *13*, 5624−5638.

(60) Abdallah, H. H.; Ishmael, H. M.; Abdullah, H. Y.; Umar, Y.; Ramasami, P. Theoretical study of the syn- and anti-conformers of 2,2′-bifuran derivatives: rotational barrier and solvent effect. *Phys. Chem. Liq.* **2019**, *57*, 174−183.

(61) Vikramaditya, T.; Lin, S.-T. Limitations of Global Hybrids in Predicting the Geometries and Torsional Energy Barriers of Dimeric Systems and the Role of Hartree Fock and DFT Exchange. *J. Comput. Chem.* **2019**, *40*, 2810−2818.

(62) Møller, C.; Plesset, M. S. Note on an Approximation Treatment for Many Electron Systems. *Phys. Rev.* **1934**, *46*, 618.



https://doi.org/10.1021/acs.jpca.1c04714
J. Phys. Chem. A XXXX, XXX, XXX−XXX

(63) Lee, C.; Yang, W.; Parr, R. G. Development of the Colle-Salvetti correlation-energy formula into a functional of the electron density. *Phys. Rev. B* **1988**, *37*, 785−789.
(64) Becke, A. D. Density-functional thermochemistry. III. The role of exact exchange. *J. Chem. Phys.* **1993**, *98*, 5648−5652.
(65) Stephens, P. J.; Devlin, F. J.; Chabalowski, C. F.; Frisch, M. J. Ab Initio Calculation of Vibrational Absorption and Circular Dichroism Spectra Using Density Functional Force Fields. *J. Phys. Chem. A* **1994**, *98*, 11623−11627.
(66) Chai, J.-D.; Head-Gordon, M. Long-range corrected hybrid density functionals with damped atom-atom dispersion corrections. *Phys. Chem. Chem. Phys.* **2008**, *10*, 6615−6620.
(67) Zhao, Y.; Truhlar, D. G. The M06 suite of density functionals for main group thermochemistry, thermochemical kinetics, non-covalent interactions, excited states, and transition element-: two new functionals and systematic testing of four M06-class functionals and 12 other functionals. *Theor. Chem. Acc.* **2008**, *120*, 215−241.
(68) Čížek, J. On the Correlation Problem in Atomic and Molecular Systems. Calculation of Wavefunction Components in Ursell-Type Expansion Using Quantum-Field Theoretical Methods. *J. Chem. Phys.* **1966**, *45*, 4256−4266.
(69) Purvis, G.; Bartlett, R. A full coupled-cluster singles and doubles model: The inclusion of disconnected triples. *J. Chem. Phys.* **1982**, *76*, 1910.
(70) Raghavachari, K.; Trucks, G. W.; Pople, J. A.; Head-Gordon, M. A fifth-order perturbation comparison of electron correlation. *Chem. Phys. Lett.* **1989**, *157*, 479−483.
(71) Dunning, T. H. Gaussian basis sets for use in correlated molecular calculations. I. The atoms boron through neon and hydrogen. *J. Chem. Phys.* **1989**, *90*, 1007.
(72) Woon, D. E.; Thom H. Dunning, J. Gaussian basis sets for use in correlated molecular calculations. III. The atoms aluminum through argon. *J. Chem. Phys.* **1993**, *98*, 1358−1371.
(73) Adler, T. B.; Knizia, G.; Werner, H.-J. A simple and efficient CCSD(T)-F12 approximation. *J. Chem. Phys.* **2007**, *127*, No. 221106.
(74) Knizia, G.; Adler, T. B.; Werner, H.-J. Simplified CCSD(T)-F12 methods: Theory and benchmarks. *J. Chem. Phys.* **2009**, *130*, No. 054104.
(75) Schwilk, M.; Usvyat, D.; Werner, H.-J. Communication: Improved pair approximations in local coupled-cluster methods. *J. Chem. Phys.* **2015**, *142*, No. 121102.
(76) Ma, Q.; Werner, H.-J. Scalable Electron Correlation Methods. 5. Parallel Perturbative Triples Correction for Explicitly Correlated Local Coupled Cluster with Pair Natural Orbitals. *J. Chem. Theory Comput.* **2018**, *14*, 198−215.
(77) Peterson, K. A.; Adler, T. B.; Werner, H.-J. Systematically convergent basis sets for explicitly correlated wavefunctions: The atoms H, He, B−Ne, and Al−Ar. *J. Chem. Phys.* **2008**, *128*, No. 084102.
(78) Weigend, F. A fully direct RI-HF algorithm: Implementation, optimised auxiliary basis sets, demonstration of accuracy and efficiency. *Phys. Chem. Chem. Phys.* **2002**, *4*, 4285−4291.
(79) Weigend, F.; Köhn, A.; Hättig, C. Efficient use of the correlation consistent basis sets in resolution of the identity MP2 calculations. *J. Chem. Phys.* **2002**, *116*, 3175−3183.
(80) Yousaf, K. E.; Peterson, K. A. Optimized auxiliary basis sets for explicitly correlated methods. *J. Chem. Phys.* **2008**, *129*, No. 184108.
(81) Werner, H.-J.; Knowles, P. J.; Knizia, G.; Manby, F. R.; Schütz, M. Molpro: a general-purpose quantum chemistry program package. *Wiley Interdiscip. Rev.: Comput. Mol. Sci.* **2012**, *2*, 242−253.
(82) Werner, H.-J.; Knowles, P. J.; Knizia, G.; Manby, F. R.; Schütz, M.; Celani, P.; Györffy, W.; Kats, D.; Korona, T.; Lindh, R. et al. *MOLPRO*, version 2018.1, a package of ab initio programs. 2018; see https://www.molpro.net.
(83) Frisch, M. J.; Trucks, G. W.; Schlegel, H. B.; Scuseria, G. E.; Robb, M. A.; Cheeseman, J. R.; Scalmani, G.; Barone, V.; Peterson, G. A.; Nakatsuji, H. et al. *Gaussian16*, revision A.03; Gaussian Inc.: Wallingford CT, 2016.


https://doi.org/10.1021/acs.jpca.1c04714
J. Phys. Chem. A XXXX, XXX, XXX−XXX